buildings

MDPI

Article

Extreme Wind Loading on Flat-Roof-Mounted Solar Arrays with Consideration of Wind Directionality

Jingxue Wang [1,*], Min Liu [2,3,*], Qingshan Yang [2,3], Yi Hui [2,3] and Shidong Nie [2]

[1] School of Soil and Water Conservation, Beijing Forestry University, Beijing 100083, China
[2] School of Civil Engineering, Chongqing University, Chongqing 400044, China
[3] Chongqing Key Laboratory of Wind Engineering and Wind Energy Utilization, Chongqing 400044, China
* Correspondence: jingxuewang@bjfu.edu.cn (J.W.); liu.min@cqu.edu.cn (M.L.)

Abstract: The assessment of extreme wind loading on solar arrays plays a significant role in ensuring their safe operation under strong winds. Therefore, this paper investigates the extreme wind loading on solar arrays mounted on a flat roof by taking into account the wind directionality effect. The estimation process is conducted by using in situ wind speeds obtained from meteorological stations and wind loading coefficients on solar arrays obtained from wind tunnel tests based on the joint probability distribution of multiple variables and their conditional probabilities. This allows a discussion regarding how the extreme wind loading of solar arrays would be affected by such factors as the uncertainty of wind loading coefficient, the structural orientation of buildings on which solar arrays are mounted, and the directional characteristics of wind speeds. Finally, a comparison among the proposed methods, considering the wind directionality in current wind loading codes, is performed. The extreme wind loading determined by multivariate extreme value theory is found to be comparable to the corresponding estimate calculated according to the independent assumption of directional extreme wind speed. The results of this study provide a valuable reference for the design of wind-resistant solar arrays that takes account of wind directionality effect.

Keywords: extreme wind loading; flat-roof-mounted solar arrays; wind directionality; probability distribution; multivariate extreme value theory

Citation: Wang, J.; Liu, M.; Yang, Q.; Hui, Y.; Nie, S. Extreme Wind Loading on Flat-Roof-Mounted Solar Arrays with Consideration of Wind Directionality. *Buildings* **2023**, *13*, 221. https://doi.org/10.3390/buildings13010221

Academic Editor: Theodore Stathopoulos

Received: 30 August 2022
Revised: 30 December 2022
Accepted: 11 January 2023
Published: 12 January 2023

1. Introduction

With the rapidly growing demand for renewable energy, construction and installation of solar arrays have been increasingly in recent years [1,2]. To reduce the area of land occupied for solar array construction while enhancing the energy efficiency of residential buildings, solar arrays are commonly installed on roofs with a certain tilt angle. Exposed to the atmospheric wind field that causes unsteady wind loads, solar arrays can be damaged by strong winds [3,4]. In this sense, the accurate assessment of extreme wind loading on solar arrays plays an essential role in the practice of structural design [3–5].

Until now, there has been plenty of literature on the wind load applied to building-mounted solar arrays [3–7]. Previous results show that the wind loading coefficients of solar arrays vary significantly by the angle of attack [3,5–7]. For example, Kopp et al. [6] performed wind tunnel tests on 12 × 12 solar arrays mounted on a 7.3 m high flat-roof building assuming where the modules tilted southwards in the northern hemisphere, the building width ran in the east–west direction, and the building length ran in the north–south direction. The results indicated that the critical wind directions for the worst minima of the pressure coefficients were northern (0°–10°), northern cornering (40°–50°), and southern (170°–180°), supposing that the approaching wind coming from north was defined as 0° and increased in a clockwise direction. Wang et al. [7] conducted wind tunnel tests to analyze the wind pressures applied to the flat-roof-mounted solar arrays in seven rows whose orientations were the same as those in the study of Kopp et al. [6] given different

angles of wind attack. According to the results, the large negative peak values of solar panels near the eastern edge are attributable to the oblique winds with its direction in the range of 40°–60°. Alrawashdeh and Stathopoulos [3] conducted a series of wind tunnel tests to examine the wind loads applied to the solar arrays mounted on flat roofs at a geometric test scale of 1:200, 1:100, and 1:50, respectively. The peak force coefficients of the panels' middle module were found to vary significantly among different wind directions. It can be concluded that the aerodynamics of building-mounted solar arrays are determined largely by the angle of wind attack.

Despite plenty of studies on the wind loading coefficients of solar arrays [3–7], no attention has been paid to how the directional characteristics of wind speed would affect the extreme wind loads applied to solar arrays. If the critical angle of wind attack for extreme wind loading coefficient is inconsistent with the dominant direction of extreme mean wind speed, there may be a significant reduction in the extreme wind loading on solar arrays. Accordingly, the cost of solar arrays construction can be reduced. Therefore, it is essential to study the extreme wind loading on building-mounted solar arrays by taking into account wind directionality effects for its optimal structural design. In addition, the directionality effect is usually accounted for by a directionality factor in engineering, which allows for a reduction in extreme wind load effects with a given mean recurrence interval (MRI) from the worst-case scenario [8,9]. A directionality factor of 0.85 is proposed in ASCE/SEI 7-16 [10]. The directionality factor should be examined for solar arrays.

This study aims to estimate the extreme wind loading applied to flat-roof-mounted solar arrays by taking into consideration actual wind directionality. The in situ wind speeds obtained from the meteorological stations in China and the extreme wind loading coefficients obtained from wind tunnel tests are adopted for this procedure. Then, a discussion is conducted regarding how the uncertainty of wind loading coefficient, the structural orientation of a building on which the solar arrays are mounted, and the characteristics of wind speed directionality would impact the extreme wind loading of solar arrays. Furthermore, a comparison is performed among different methods set out in current wind loading codes by considering the directionality effect to determine the extreme wind loads applied to building-mounted solar arrays.

2. Probabilistic Modelling of Extreme Wind Loading on Solar Arrays with Consideration of Wind Directionality

2.1. Probabilistic Modelling Methodology

The extreme wind loading w_i at the ith wind direction for solar arrays is expressed as:

$$w_i = \frac{1}{2}\rho v_i^2 c_i \ (i = 1, 2, \ldots, n) \tag{1}$$

where ρ represents air density; v_i indicates the yearly maximum mean wind speed at the ith direction; and c_i denotes the extreme wind loading coefficient of solar arrays at the ith direction, which is independent of wind speed in case of strong wind.

To calculate the extreme wind loading of solar arrays, the directional extreme wind loading coefficient c_i is considered to be a deterministic value or random variable. It is assumed that when the extreme wind loading coefficient c_i is deterministic, the yearly maximum mean wind speed v_{iw} corresponding to load level w at the ith direction can be calculated by using Equation (1) as:

$$v_{iw} = \sqrt{2w/\rho c_i}(i = 1, 2, \ldots, n) \tag{2}$$

The cumulative distribution function (CDF) of extreme wind loading $\Psi_w(w)$ that considers wind directionality is expressed as:

$$\Psi_w(w) = F_v(v_{1w}, v_{2w}, \cdots v_{nw}) \tag{3}$$

where $F_v(v_{1w}, v_{2w}, \cdots v_{nw})$ represents the joint cumulative distribution function (JCDF) of directional yearly maximum mean wind speeds, as modeled by using Gaussian copula [11]. The process of estimating the JCDF of multivariate extremes via Gaussian copula is detailed in the Appendix A. The MRI of load level w is $R = 1/[1 - \Psi_w(w)]$ [12].

When the extreme wind loading coefficient c_i is treated as a random variable, the CDF of extreme wind loading can be calculated according to the theory of conditional probability [13] as follows:

$$\Psi_w(w) = \int \cdots \int F_c(c_1|v_1, c_2|v_2, \ldots, c_n|v_n) f_v(v_1, v_2, \cdots v_n) \mathrm{d}v_1 \mathrm{d}v_2 \cdots \mathrm{d}v_n \quad (4)$$

where $f_v(v_1, v_2, \cdots v_n)$ represents the joint probability density function (JPDF) of directional yearly maximum mean wind speeds, and $F_c(c_1|v_1, c_2|v_2, \ldots, c_n|v_n)$ indicates the JCDF of extreme wind loading coefficients. It is usually assumed that $c_i|v_i = 2w/\rho v_i^2$ $(i = 1, 2, \ldots, n)$ are mutually independent [13,14]. Therefore, Equation (4) is rewritten as:

$$\Psi_w(w) = \int \cdots \int \Psi_{c_1}(c_1|v_1)\Psi_{c_2}(c_2|v_2) \cdots \Psi_{c_n}(c_n|v_n) f_v(v_1, v_2, \cdots v_n) \mathrm{d}v_1 \mathrm{d}v_2 \cdots \mathrm{d}v_n \quad (5)$$

where $\Psi_{c_i}(c_i|v_i)$ represents the CDF of c_i. For improved computational efficiency, the multiple integration in Equation (5) is estimated by performing Monte Carlo simulation, as shown in the study of Liu et al. [13]. The samples of v_i $(i = 1, 2, \ldots, n)$ are first generated according to their JPDF. Then, the corresponding $\Psi_{c_i}(c_i|v_i)$ is calculated. The $\Psi_w(w)$ is obtained by the ensemble average.

When the directional yearly maximum mean wind speeds are independent of each other, the CDF of yearly maximum wind loading can be calculated as:

$$\Psi_w(w) = \Psi_{w_1}(w)\Psi_{w_2}(w) \cdots \Psi_{w_n}(w) \quad (6)$$

$$\Psi_{w_i}(w) = \int_0^\infty \Psi_{c_i}(c_i|v_i)\varphi_{v_i}(v_i)\mathrm{d}v_i \quad (7)$$

where $\varphi_{v_i}(v_i)$ represents the PDF of yearly maximum mean wind speed at the ith direction, and $\Psi_{w_i}(w)$ refers to the corresponding CDF of extreme wind loading. It can be calculated through the closed-form formulation proposed in the study of Chen [15].

2.2. Directional Extreme Wind Speed Model

The wind speed data used in this study are sourced from the National Meteorological Information Center, China (http://data.cma.cn/data/ accessed on 17 June 2020). The wind speeds, as measured in Jinan city of Shandong province in China from 1 January 1969, to 31 December 2007, are analyzed. The reference height is set to 10 m, and the average interval of mean wind speed is set to 10 min. In the original data set, the wind speeds are divided into 16 directional sectors. Both daily maximum mean wind speed and the corresponding wind direction are publicly accessible.

On the basis of the daily maximum mean wind speed included in the data set, the directional yearly maximum mean wind speed data in eight sectors is processed to represent the directions of N, NE, E, SE, S, SW, W, and NW, respectively. If the wind load is particularly sensitive to wind direction, this can be divided into more directional sectors. Since only daily maximum wind speeds are included in the original data set, it is likely to encounter the "masking" problem of directional yearly maximum wind speed [11]. After checking, only one directional yearly maximum mean wind speed is found to be masked in the selected data set. Herein, the masked yearly maximum mean wind speed v_β at direction β is estimated on the basis of the corresponding values at neighboring direction γ by $v_\beta = v_\gamma \cos(\beta - \gamma)$, where $|\beta - \gamma| < \pi/2$, and v_γ indicates the yearly maximum mean wind speed at the direction γ [13,16].

In order to calculate the CDF of yearly maximum mean wind speed, the 39 directional yearly maximum mean wind speed data in each sector are first ranked in ascending order.

Then, the empirical probability of non-exceedance of the *i*th wind speed is calculated by $(i - 0.44)/(N + 0.12)$ [17], where N represents the number of total yearly maximum wind speed samples in each sector. On the basis of the empirical CDF, the marginal CDF of directional yearly maximum mean wind speed is fitted to the Gumbel distribution. Given a specific mean recurrence interval (MRI), Figure 1a shows the directional yearly maximum mean wind speeds (blue lines) and the non-directional yearly maximum mean wind speeds (red circles), as obtained from the JPDF by Gaussian copula through Equations (A1) and (A2). Since a 25-year MRI is recommended in the code of practice for the design of photovoltaic power station GB 50797-2012 [18], and a 50-year MRI is routinely adopted for the main wind force resisting system, the extreme wind speeds with MRIs of both 25 and 50 years are calculated. The non-directional yearly maximum mean wind speeds are 21.3 and 22.7 m/s, corresponding to 25-year and 50-year MRIs, respectively. The three highest wind speeds among the eight directions arise in the E, NW, and S directions, the values of which reach 19.0, 18.3, and 17.3 m/s, respectively, corresponding to 25-year MRI. For 50-year MRI, their values are 20.4, 20.1, and 18.8 m/s, respectively. Figure 1b shows the coefficient of variation (CoV) in directional yearly maximum mean wind speed. The value of CoV varies from 17.3% to 29.9%, with the maximum CoV arising in the SE direction.

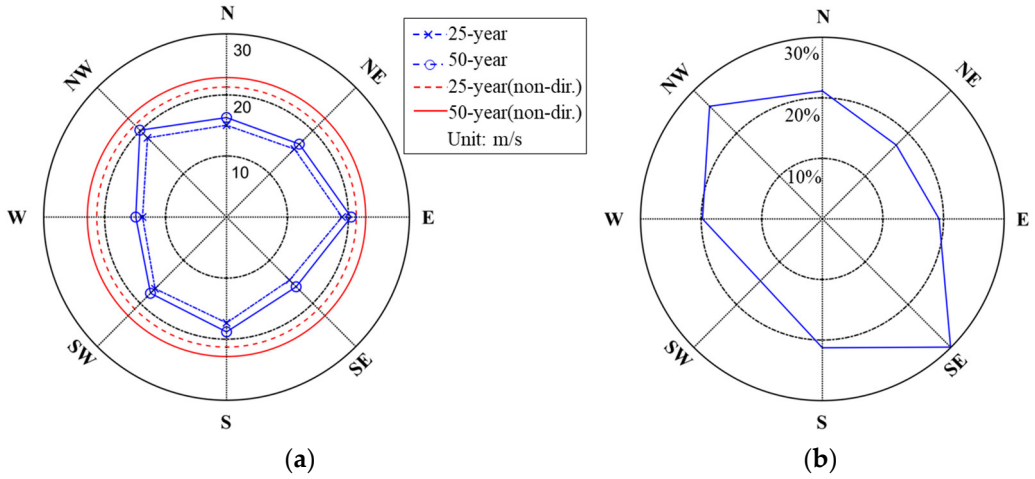

Figure 1. Extreme wind speeds with different MRIs and the CoV along each direction in Jinan, China: (**a**) Wind speeds of different MRIs; (**b**) CoV.

Table 1 shows the correlation coefficients of yearly maximum mean wind speed between different wind directions. The largest correlation coefficient of 0.63 arises between E and SW, whose typical dependence structure pattern is illustrated in Figure 2. As shown in Figure 2a, the JPDF of wind speeds in the E and SW directions are effectively modeled by Gaussian copula. The elliptical shape in Figure 2b shows the dependence relationship between two corresponding underlying Gaussian variables. For brevity, the correlation coefficients of underlying Gaussian variables are not provided here.

Table 1. Correlation coefficients of wind speeds between different wind directions in Jinan, China.

Direction	N	NE	E	SE	S	SW	W	NW
N	1							
NE	0.19	1						
E	0.43	0.21	1					
SE	−0.10	−0.05	0.13	1		Sym.		
S	0.23	0.11	0.36	0.44	1			
SW	0.39	0.26	0.63	0.26	0.27	1		
W	0.18	0.09	0.31	−0.17	−0.03	0.11	1	
NW	0.37	0.27	0.54	0.17	0.27	0.51	0.34	1

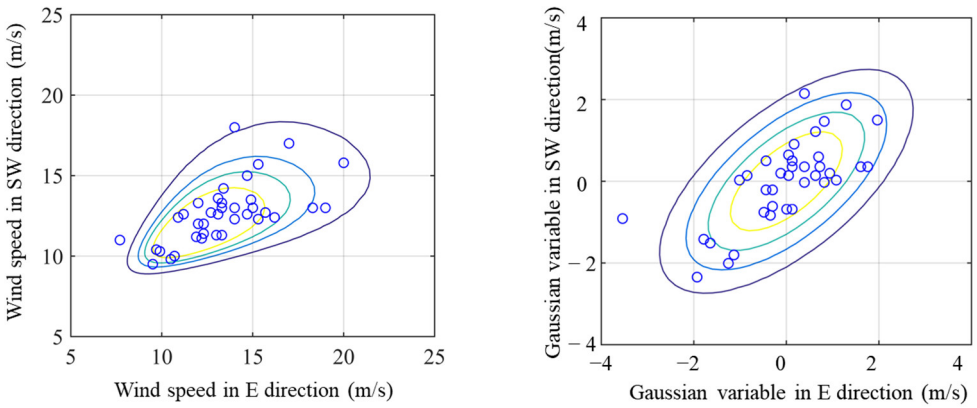

Figure 2. Dependence structure pattern and contour of JPDF of yearly maximum mean wind speeds between E and SW directions in Jinan, China: (**a**) Wind speed; (**b**) Gaussian variable.

Figure 3 shows the CDF of non-directional yearly maximum mean wind speed Ψ_v, as determined by the multivariate extreme model through Gaussian copula. On the basis of the assumption that the mean wind speeds in different wind directions are independent and fully correlated, the CDFs are, respectively, denoted as $\Psi_{v,ind.}$ and $\Psi_{v,fullcor.}$, as shown in the same figure. It can be seen clearly that Ψ_v is close to one assuming independent $\Psi_{v,ind.}$ This is especially evident for higher wind speeds. For a given MRI, the CDF of yearly maximum mean wind speed, as obtained by means of the fully correlated assumption $\Psi_{v,fullcor.}$, is smaller than Ψ_v and $\Psi_{v,ind.}$. The 25- and 50-year non-directional mean wind speeds obtained by using the multivariate model Ψ_v are 21.3 and 22.8 m/s, respectively, which is consistent with the red dashed and solid circles in Figure 1a. As shown in this figure, the non-directional wind speed exceeds the largest directional yearly maximum mean wind speed given the same MRI. This is attributed to the three dominant wind directions with a comparable wind speed, i.e., E, NW, and S, as well as the weak correlation between them, as shown in Table 1.

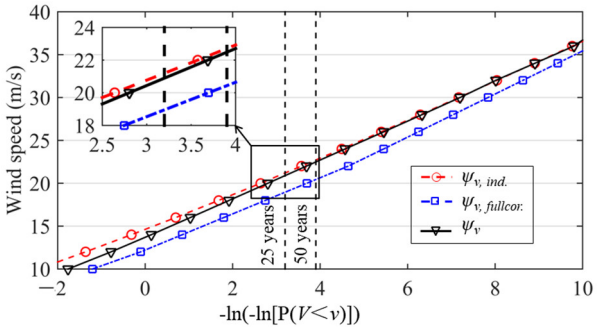

Figure 3. CDF of yearly maximum mean wind speed in Jinan, China.

2.3. Extreme Wind Loading Coefficients of Solar Arrays

Herein, an investigation is conducted by using the coefficients of extreme wind loading applied to the flat-roof-mounted solar arrays in open terrain during the wind tunnel tests conducted by Wang et al. [7]. Figure 4 shows the dimensions of the experimental model with a geometric scale of 1/50. It is assumed that the model is located in the northern hemisphere. In this case, the solar arrays tilt towards the south. The basic unit is referred to as a "module", and seven modules comprise a "panel" sized 40 mm (W) × 140 mm (L) (in model-scale, hereafter). Three panels (denoted by A–C) constitute one row, and seven rows comprise an "array", i.e., rows 1 to 7, with a space d of 24 mm. The modules in each row are numbered 1–7, 8–14, and 15–21 for panels A, B, and

C, respectively. For the sake of simplicity, in the following discussion, the module is designated by (row number-module number). They are mounted on a flat-roof building sized 520 mm (D) × 525 mm (B) × 400 mm (H). The angle of building orientation α is defined as 0° when the building's depth (D) is in the north–south direction and the width (B) is in the east–west direction. It increases with clockwise rotation of the building together with the solar arrays. The reference height is 400 mm for the wind tunnel test. The tilt angle β of the solar arrays is 15°, and their thickness is 3 mm. The setback is 52.5 mm from the solar arrays to the roof edge. There are eight pressure taps deployed on the upper/lower surface of each module. The resultant net pressures can be obtained according to the difference between upper and lower surface pressures. As for the wind loading coefficients on each module, they are obtained from the area-averaged calculation of net pressures by taking into account the tributary areas of pressure taps. As there are different approaching wind directions examined in the experiments, eight wind directions θ varying from 0° to 360° with a 45° increment are selected for analysis. For each testing direction, the duration of wind pressure record is 360 s in model scale, corresponding to ten 10 min samples in full scale, with a time scale of 3/50.

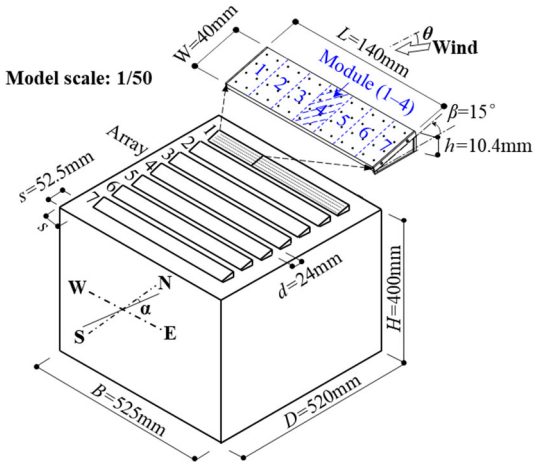

Figure 4. Experimental model of flat-roof-mounted solar arrays (NOTE: The module is designated by (row number-module number)).

On the basis of ten samples of extreme wind loading coefficients of each module, the probability distribution is determined by fitting with a Gumbel distribution, whose mode and dispersion are estimated by adopting the best linear unbiased estimator (BLUE) method [19]. The use of a moment-based Hermite model is also worth considering when the number of samples is small [20,21]. Considering Module (4-2) as an example, Figure 5 shows the probability distribution of extreme wind loading coefficients (suction) as determined when the angle of wind attack θ = 0°, 45°, 90°, 135°, and 180°. It is found out that the largest suction occurs when θ = 0°, rather than at other angles of attack. In the practice of wind engineering, there are two percentiles of the Gumbel distribution commonly used for the representation of extreme wind loading coefficient: 57% and 78% [22]. For the Gumbel distribution, the 57% and 78% percentiles correspond to the mean and mean plus 0.64 times standard deviation, respectively. Figure 6 shows the extreme wind loading coefficients corresponding to the 78% percentile $C_{78\%}$ of all the solar arrays when wind direction θ = 0°, 45°, 135°, and 180°. It can be seen from the figure that the magnitude of extreme wind loading coefficients is more significant in the direction θ = 0° than in other cases. Although the results of 57% percentile $C_{57\%}$ are not presented for brevity, their difference in determining the final extreme wind load will be discussed in Section 3.1.

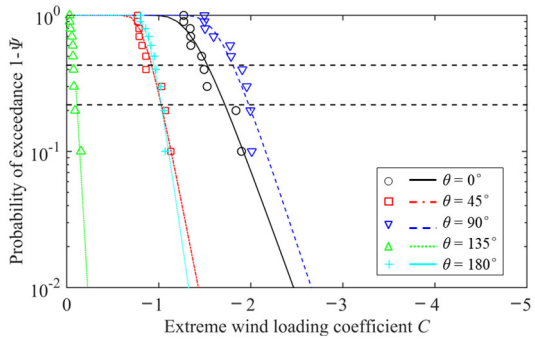

Figure 5. Probability distribution of extreme wind loading coefficients of Module (4-2) for different wind directions.

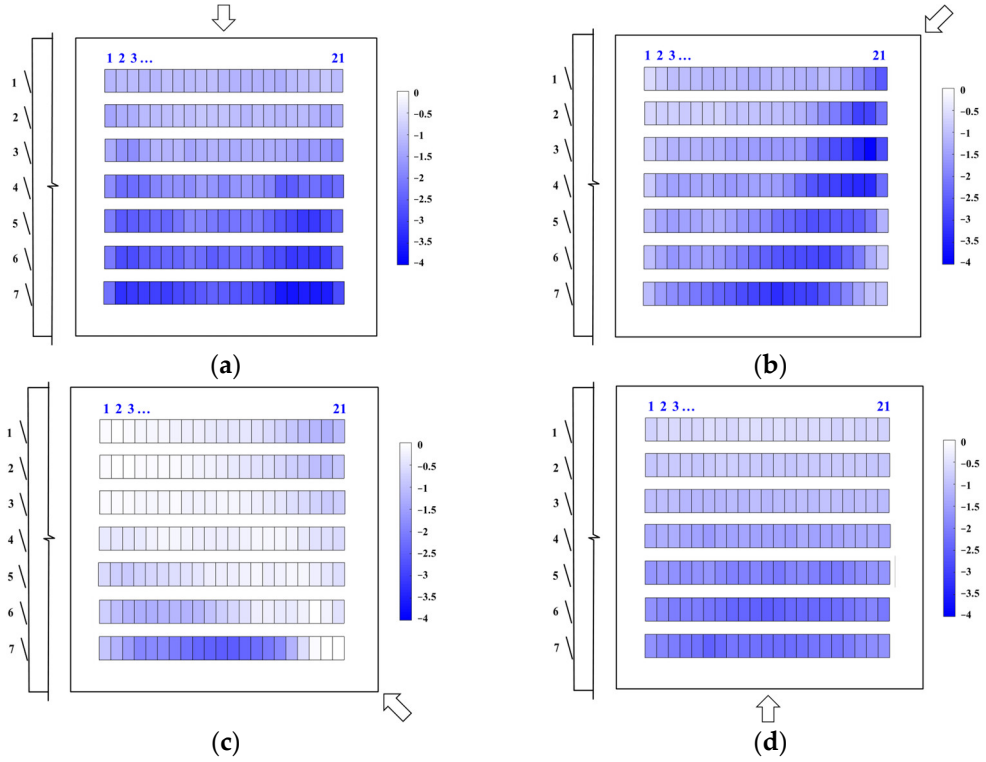

Figure 6. Contours of extreme wind loading coefficients of solar arrays corresponding to 78% percentile $C_{78\%}$: (**a**) $\theta = 0°$; (**b**) $\theta = 45°$; (**c**) $\theta = 135°$; and (**d**) $\theta = 180°$.

3. Results and Discussions

In this section, the extreme wind loading applied to flat-roof-mounted solar arrays is presented by taking account of the directionality effect. Firstly, a discussion is conducted regarding a number of factors which may cause a difference in the directionality effect, including the uncertainty of extreme wind loading coefficients, building orientation, and the characteristics of wind speed directionality. Secondly, in order to find a rational method for solar arrays, a comparison is performed among the different methods specified in the current wind loading codes by considering the directionality effect.

3.1. Effect of Uncertainty of Extreme Wind Loading Coefficients

It was reported that the directionality characteristics of extreme wind loading can be affected by the uncertainty of extreme wind loading coefficients at different angles of attack [14]. In this study, the extreme wind loading W_m is calculated by using the multivariate extreme model as well as Equations (3) and (4) in three different cases of

extreme wind loading coefficients: 57% percentile $C_{57\%}$, 78% percentile $C_{78\%}$, and random variable C_r. It is noted that the random extreme wind loading coefficient C_r is not directly calculated but regarded as a random variable when calculating the CDF of extreme wind loading on solar arrays.

Figure 7 shows how the uncertainty of extreme wind loading coefficients makes a difference in the exceedance probability of the extreme wind loading W_m on some particular modules given the building orientation of $\alpha = 0^\circ$ in Jinan, China. It can be found out that the extreme wind loading W_m based on random extreme wind loading coefficient C_r ranges between the results by adopting the extreme wind loading coefficients $C_{57\%}$ and $C_{78\%}$. With regard to the 25-year MRI, the extreme wind loading W_m, as determined by the random extreme wind loading coefficient C_r is comparable to that obtained by using the 57% percentile extreme wind loading coefficient $C_{57\%}$ for Module (1–4). However, the corresponding value for Module (4–8) is in the middle of the results obtained by using $C_{57\%}$ and $C_{78\%}$. As MRI increases, the corresponding value tends to become comparable to that calculated by using $C_{78\%}$ for both the modules. Notably, this pattern is determined by the CoV of extreme wind speed and extreme wind loading coefficients. Similar conclusions have been drawn in the study of Chen and Huang [22] and that of Zhang and Chen [14]. Figure 8 further shows how the uncertainty of extreme wind loading coefficients would cause an impact on the extreme wind loading on all the modules of the solar arrays. It can be seen from the figure that the distributions of extreme wind loading are highly similar when the extreme wind loading coefficients $C_{57\%}$, $C_{78\%}$, and C_r are used. Module (3-2) shows the largest magnitude of extreme wind loading in these three cases. The corresponding mean values of extreme wind loading for all the modules are -0.61, -0.65, and -0.63 kN/m^2, respectively.

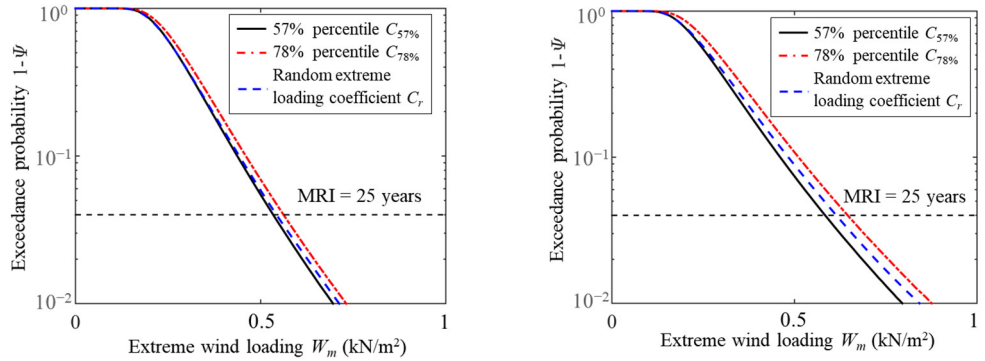

Figure 7. Exceedance probability of extreme wind loading W_m on representative solar modules with building orientation $\alpha = 0^\circ$ in Jinan, China: (**a**) Module (1–4); (**b**) Module (4–8).

In the current codes and standards, the directionality factor k_d is commonly used to indicate the reduction effect of wind direction on wind loads. It can be calculated through the following equation:

$$k_d = \frac{W_m}{W_w} \tag{8}$$

where W_w represents the worst case of extreme wind loading when the non-directional wind speed $v_{non\text{-}dir}$. and the maximum extreme wind loading coefficients among the eight wind directions C_{max} are adopted, which means $W_w = \frac{1}{2}\rho v^2_{non-dir.} C_{max}$. Figure 9a,b show the distribution of directionality factor k_d of all modules when extreme wind loading coefficients $C_{57\%}$ and $C_{78\%}$ are adopted. According to the results, the directionality factors of the same module are basically the same under these two scenarios. It is discovered that the modules in the western regions have larger values than those in the eastern regions. The mean directionality factor is 0.72 for all modules, which is smaller than the value of 0.85

that is commonly used for the generic components and claddings specified in ASCE/SEI 7-16 [10].

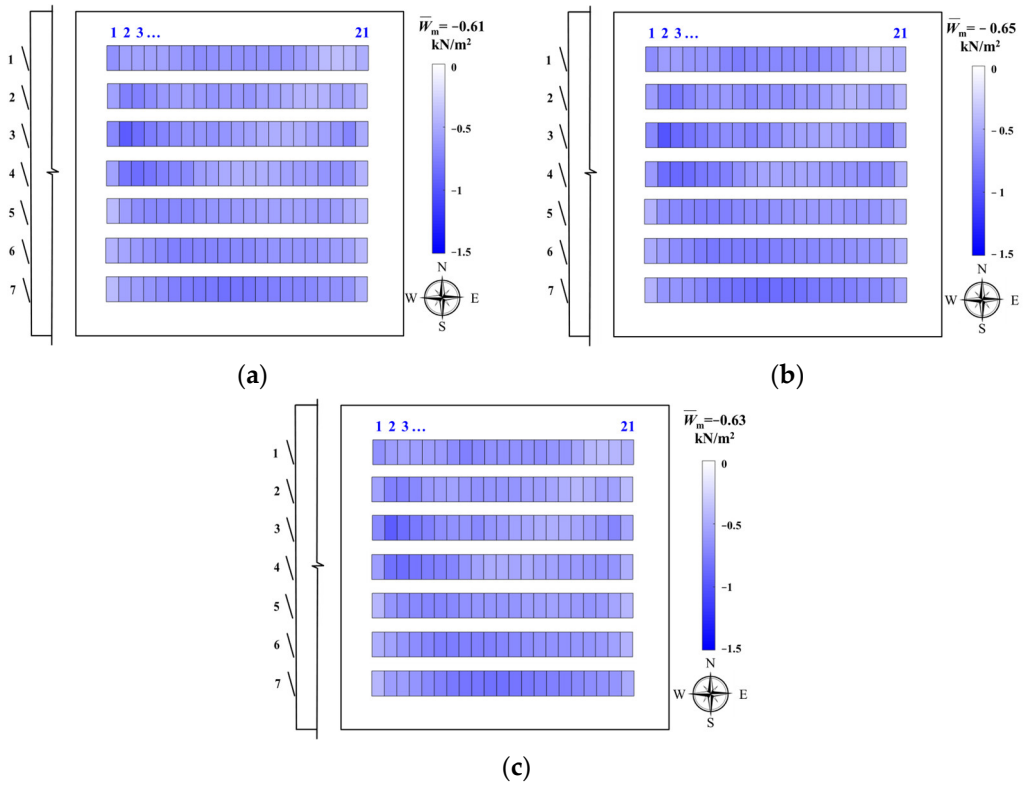

Figure 8. Distributions of extreme wind loading W_m on the solar arrays with building orientation α = 0° in Jinan, China, given different extreme wind loading coefficients: (**a**) 57% percentile $C_{57\%}$; (**b**) 78% percentile $C_{78\%}$; and (**c**) Random wind loading coefficient C_r.

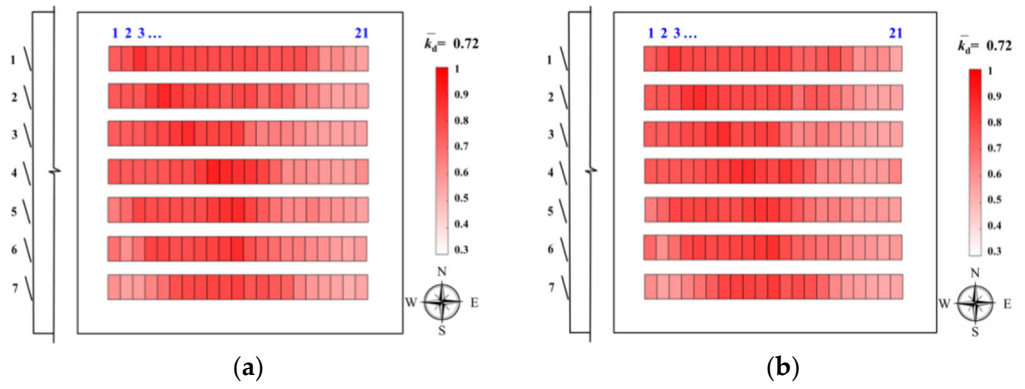

Figure 9. Distributions of directionality factor k_d for solar arrays with building orientation α = 0° in Jinan, China, given different extreme wind loading coefficients: (**a**) 57% percentile $C_{57\%}$; (**b**) 78% percentile $C_{78\%}$.

3.2. Effect of Building Orientation

The building orientation affects not only aerodynamic characteristics but also the extreme wind loading coefficient of solar arrays mounted on the roofs, which further determines the final extreme wind load applied to solar arrays. In this section, it is examined how building orientation affects the extreme wind load applied to solar arrays by taking into consideration the directionality effects, which involves three different building orientations α = 0°, 45°, and −45°. Figure 10 shows the extreme wind loading of solar arrays installed

in Jinan, China, as determined when the building orientation α = 45° and −45° and by using the 78% percentile extreme wind loading coefficients $C_{78\%}$. Figure 8b shows the corresponding results for building orientation α = 0°. Through a comparison with Figures 8b and 10, it can be found out that the distribution of extreme wind load applied to solar arrays varies significantly among different building orientations: α = 0°, 45°, and −45°. When building orientation α = 0°, Module 2 in Row 3 shows the largest magnitude of extreme wind loading, as can be seen from Figure 8b. When building orientation α = 45°, Module 20 in Row 3 has the largest magnitude, as shown in Figure 10a. When building orientation α =−45°, as shown in Figure 10b, the largest magnitude of extreme wind load is reached by Modules 16–20 in Row 7. The mean values of extreme wind load applied to all modules are −0.65, −0.70, −0.61 kN/m^2 when building orientation α = 0°, 45°, and −45°, respectively. Therefore, a conclusion can be drawn that building orientation makes a significant difference to the distribution of extreme wind load applied to solar arrays.

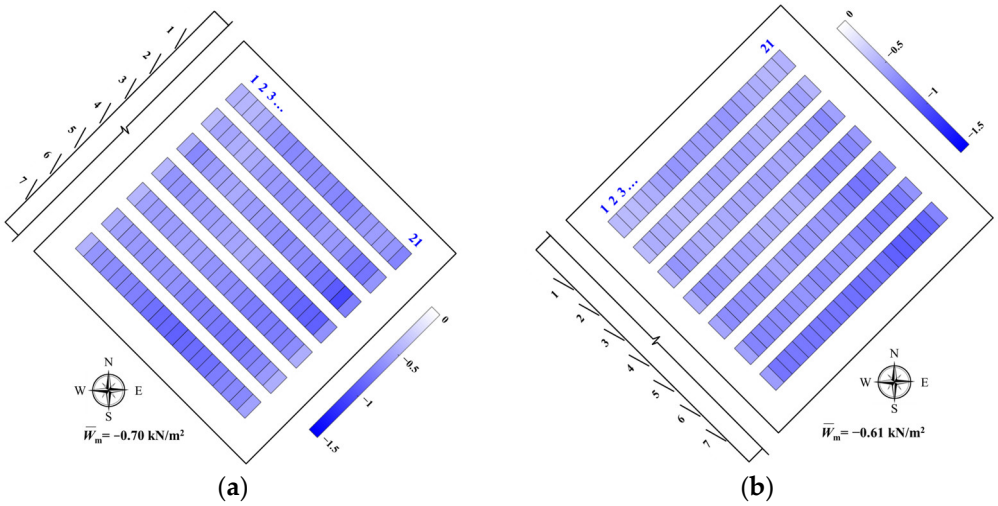

Figure 10. Distributions of extreme wind loading W_m of solar arrays installed in Jinan, China, with different building orientations: (**a**) α = 45°; (**b**) α = −45°.

Figure 11a,b show the directionality factors of solar arrays installed in Jinan, China, when building orientation α = 45° and −45° based on a 78% percentile extreme wind loading coefficient $C_{78\%}$. When building orientation α = 45°, as shown in Figure 11a, most of the modules in the western regions have a larger directionality factor, which results in a less significant reduction in extreme wind loading when directionality effect is taken into account. A similar trend can be observed when building orientation α = 0°, as shown in Figure 9b. According to Figure 11b, the modules in the southeast have a larger directionality factor when building orientation α = −45°. The mean values of directionality factors for all the modules are 0.72, 0.73, and 0.67 when building orientation α = 0°, 45°, and −45°, respectively.

3.3. Effect of Wind Speeds with Different Directionality Characteristics

It is known that the directionality characteristics of wind speed vary from place to place. To verify the effect of wind speed directionality characteristics on the extreme wind loading of solar arrays, the wind speeds as measured in Beijing are used for comparisons with those measured in Jinan. The directional extreme wind speed model is processed through the same process as in Jinan city, as detailed in Section 2.2. The relevant results can be found in the study of Liu et al. [13]. As indicated by Liu et al. [13], the non-directional wind speed with MRI of 25 years is 25.2 m/s at a reference height of 10 m, which is relatively larger than the corresponding value of 21.3 m/s in Jinan. The wind speed in the N direction is the highest, while those in the NW, W, and SW directions are comparable and higher than in the SE, E, and NE directions.

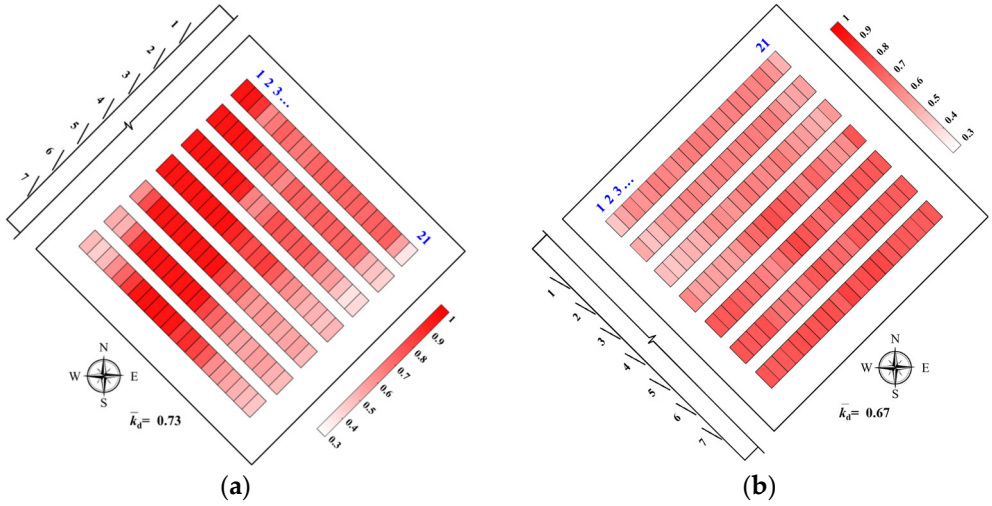

Figure 11. Distributions of directionality factor k_d for solar arrays installed in Jinan, China, with different building orientations: (**a**) $\alpha = 45°$; (**b**) $\alpha = -45°$.

Figure 12a,b show the extreme wind loading of solar arrays when building orientation $\alpha = 45°$ in Jinan and Beijing, respectively. The mean value of extreme wind loading of solar arrays installed in Beijing is -0.93 kN/m^2, which is clearly higher than the corresponding value of -0.70 kN/m^2 in Jinan. Additionally, Figure 12b shows that the modules near the west and south regions have the highest extreme wind load, given the wind speed as measured in Beijing. However, there are a small number of modules in the east and south showing the highest extreme wind load in Jinan, as can be seen from Figure 12a. Figure 13a,b show the directionality factors in Jinan and Beijing when structure orientation $\alpha = -45°$. The mean value of directionality factor in Beijing is 0.73, which is comparable to that in Jinan. Nevertheless, the distribution of directionality factor varies considerably between these two regions, which indicates the significant difference in the characteristics of wind speed directionality.

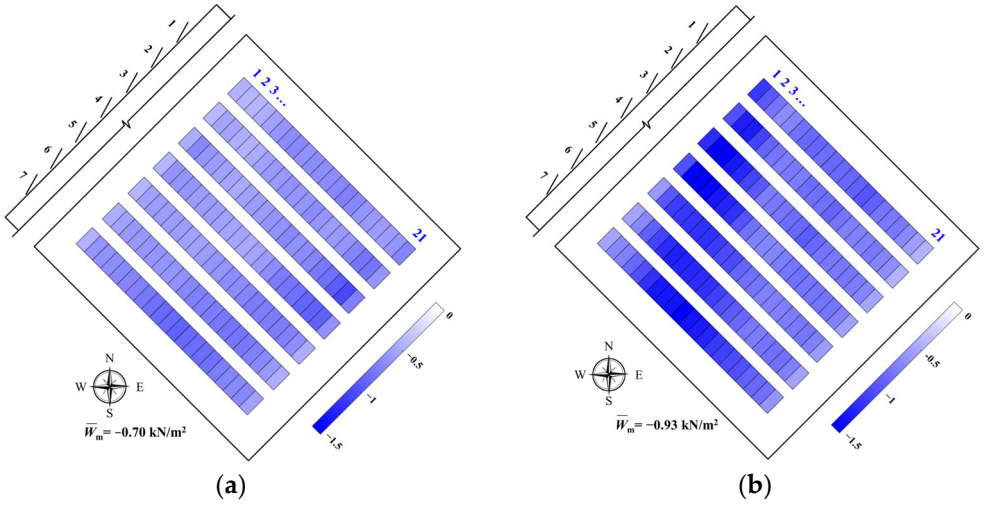

Figure 12. Distributions of extreme wind loading W_m of solar arrays with building orientation $\alpha = 45°$ in different regions: (**a**) Jinan, China; (**b**) Beijing, China.

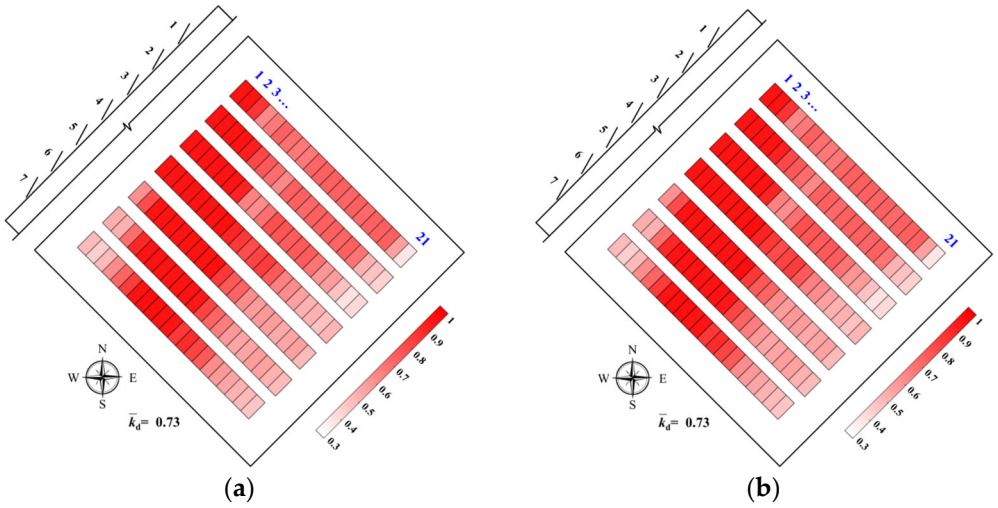

Figure 13. Distributions of directionality factor k_d on solar arrays with building orientation $\alpha = 45°$ at different locations: (**a**) Jinan, China; (**b**) Beijing, China.

3.4. Discussions on Methods for Considering Directionality Effect

There are several methods in current wind loading codes and standards that take into account the directionality effect. The directionality factor of 0.85 is proposed in ASCE/SEI 7-16 [10]. In line with the Australian/New Zealand standard [23], it is assumed that there is full correlation between different wind direction sectors. The directionality effect is ignored for the claddings and components, as mentioned in the Architectural Institute of Japan (AIJ) recommendations [24].

Figure 14 shows the probability of exceedance for the extreme wind loading applied to Module (2–4) when building orientation $\alpha = 0°$ in Jinan, China. The results, as obtained under three different scenarios—by considering the real correlation in line with multiple extreme theory W_m, full-correlation assumption W_f, and independent assumption W_i of directional extreme wind speeds—are included. Two dominant wind directions, i.e., NW and E, are identified by comparing the probability of exceedance of extreme wind loading in each wind direction. The extreme wind loading is -0.71 kN/m^2 when consideration is given to the real correlation of directional extreme wind speed W_m with an MRI of 25 years. The corresponding values determined by full-correlation and independent assumptions, i.e., W_f and W_i, are -0.62 and -0.72 kN/m^2, respectively. Apparently, the magnitude of extreme wind load determined by multiple extremes W_m is larger than the corresponding value based on the full-correlation assumption W_f, as made in the Australian/New Zealand standard [23], despite being comparable to the values based on the independent assumption W_i, as made in the case of this study.

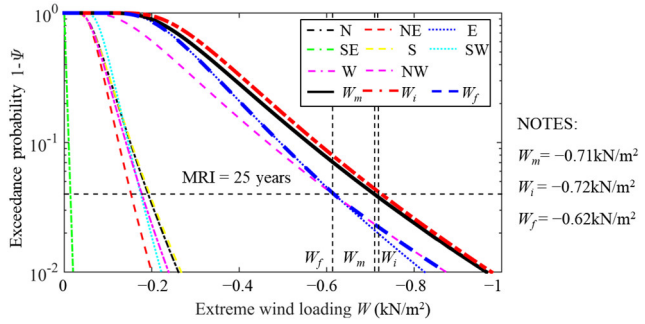

Figure 14. Exceedance probability of extreme wind loading on Module (2–4) with building orientation $\alpha = 0°$ located in Jinan, China.

Table 2 shows the mean value of extreme wind loading applied to solar arrays installed in Jinan, China, by using different methods. Three different building orientations are taken into consideration: $\alpha = 0^\circ$, 45°, and -45°. Again, the extreme wind loading based on the independent assumption W_i is comparable to that as determined when real correlation is considered by multivariate extreme model W_m. The directionality factors $k_d = W_m/W_w$ are 0.72, 0.72, and 0.67, respectively, all of which are smaller than the value of 0.85, as proposed for the generic components and claddings in ASCE/SEI 7-16 [10]. As for the corresponding results of full correlation assumption W_f, as proposed in Australian/New Zealand standard [23], they tend to be smaller. The advantage of the independent assumption made in this study is basically consistent with the conclusions drawn in the study of Liu et al. [13], as recommended for use in the future.

Table 2. Comparisons of mean value of extreme wind loading on solar arrays located in Jinan, China, using different methods (Units: kN/m^2).

Orientation α	Worst Case W_w	Multivariate Extreme Model W_m	Independent W_i	Full-Correlated W_f	Directionality Factor $k_d = W_m/W_w$
$\alpha = 0^\circ$	−0.91	−0.65	−0.66	−0.60	0.72
$\alpha = 45^\circ$		−0.70	−0.66	−0.60	0.72
α =- 45°		−0.61	−0.62	−0.56	0.67

4. Conclusions

In the present study, the probabilistic estimation of extreme wind loading of flat-roof-mounted solar arrays is addressed by considering the directionality effects. Then, a discussion is conducted regarding how the uncertainty of extreme wind loading coefficient, building orientation, and the characteristics of wind speed directionality would affect the extreme wind loading of solar arrays. The main findings are summarized as follows:

(1) The extreme wind loading of solar arrays, as determined by considering the characteristics of wind directionality, could differ when deterministic extreme wind loading coefficients are used, i.e., 57% and 78% percentiles, as well as a random variable. The extreme wind loading coefficients corresponding to the 78% percentile are recommended for the estimation of extreme wind load applied to solar arrays for a greater safety of design.

(2) The distribution of extreme wind loading and directionality factor of solar arrays varies by building orientations and the characteristics of wind directionality. If the critical angle of attack for large extreme loading coefficient is consistent with the direction of high wind speed, there would be a sharp rise in the extreme wind loading of solar arrays.

(3) The extreme wind loading under the real correlation of directional wind speed is found to be comparable to the values based on the independent assumption, but larger than the corresponding results of the full-correlation assumption.

(4) In most cases, the directionality factor of solar arrays is smaller than the value of 0.85, as recommended for the generic components and claddings specified in ASCE/SEI 7-16.

Author Contributions: Conceptualization, J.W. and M.L.; methodology, M.L.; software, J.W. and M.L.; validation, J.W. and M.L.; investigation, J.W. and M.L.; resources, Q.Y.; writing—original draft preparation, J.W.; writing—review and editing, M.L., Q.Y., Y.H. and S.N.; visualization, Y.H.; supervision, Q.Y.; project administration, J.W., M.L. and Q.Y.; funding acquisition, J.W., M.L. and Q.Y. All authors have read and agreed to the published version of the manuscript.

Funding: This study is supported by Fundamental Research Funds for the Central Universities (2021ZY48), National Natural Science Foundation of China (No. 32101589), Postdoctoral Research Completion and Staying in Chongqing Starting up Foundation (2020LY08), China Postdoctoral Science Foundation (2021M690417), and the 111 Project of China (B18062).

Data Availability Statement: Not applicable.

Acknowledgments: The discussion with Yukio Tamura in Chongqing University and Tokyo Polytechnic University is really appreciated.

Conflicts of Interest: The authors declare no conflict of interest.

Appendix A

The JCDF of multivariate extremes, i.e., multiple yearly maximum mean wind speed, can be modeled by using Gaussian copula. It is expressed as:

$$F_x(x_1, x_2, \ldots, x_n) = G_y(y_1, y_2, \ldots, y_n) \tag{A1}$$

where $F_x(x_1, x_2, \ldots, x_n)$ represents the JCDF of multiple extremes $x_1, x_2, \ldots, x_n$; and $G_y(y_1, y_2, \ldots, y_n)$ indicates the JCDF of standard Gaussian variables $y_1, y_2, \ldots, y_n$, with zero mean vector and covariance matrix Σ, where $\Sigma_{ii} = 1$ and $\Sigma_{ij} = \Sigma_{ji} = \rho_{ij}$, which is the correlation coefficient between y_i and y_j.

The extreme variable x_i and standard Gaussian variable y_i can be related to each other by the monotonic translation function as follows:

$$\left(x_i - \mu_{x_i}\right)/\sigma_{x_i} = \Psi_{x_i}^{-1}[\Phi(y_i)] = g_i(y_i) \tag{A2}$$

where μ_{x_i} and σ_{x_i} represent the mean and standard deviation (STD) of x_i; and $\Psi_{x_i}(x_i)$ and $\Phi(y_i)$ are the corresponding CDFs of x_i and y_i, respectively.

The correlation coefficient between x_i and x_j, i.e., $\zeta_{ij} = \left[E(x_i x_j) - \mu_{x_i}\mu_{x_j}\right]/\sigma_{x_i}\sigma_{x_j}$ is related to that of Gaussian variables y_i and y_j, as shown in [23]:

$$\zeta_{ij} = \int_{-\infty}^{\infty}\int_{-\infty}^{\infty} g_i(y_i) g_j(y_j)\, \Phi\left(y_i, y_j; \rho_{ij}\right) \mathrm{d}y_i \mathrm{d}y_j \tag{A3}$$

where $\Phi\left(y_i, y_j; \rho_{\mathrm{ij}}\right)$ represents the JPDF of the bivariate Gaussian distribution. Some properties of ζ_{ij} have been demonstrated in the literature [24–26].

The Gumbel distribution (Type I extreme distribution) is frequently used to model the distribution of yearly maximum mean wind speed x_i as follows:

$$\Psi_{x_i}(x_i) = \exp\left[-\exp\left(-\frac{x_i - m_i}{\delta_i}\right)\right] \tag{A4}$$

where m_i represents mode coefficient, and δ_I indicates dispersion coefficient. The mean and STD are, respectively, $\mu_{x_i} = m_i + \gamma\delta_i$ and $\sigma_{x_i} = \delta_i\pi/\sqrt{6}$, where $\gamma = 0.5772$ is the Euler constant.

Thus, the translation function for the Gumbel I distribution can be expressed as:

$$g_i(y_i) = -\frac{\sqrt{6}}{\pi}(\ln\{-\ln[\Phi(y_i)]\} + \gamma) \tag{A5}$$

In the above equation, it is worth noting that the distribution parameters of the Gumbel distribution make no difference to the relationship between the correlation coefficient of the Gumbel-distributed variables nor that of the standard Gaussian variable [25,27]. It can be approximated as follows [25]:

$$\rho_{ij} = \zeta_{ij}\left(1.064 - 0.069\zeta_{ij} + 0.005\zeta_{ij}^2\right) \tag{A6}$$

References

1. Al-Quraan, A.; Al-Mahmodi, M.; Al-Asemi, T.; Bafleh, A.; Bdour, M.; Muhsen, H.; Malkawi, A. A new configuration of roof photovoltaic system for limited area applications-A case study in KSA. *Buildings* **2022**, *12*, 92. [CrossRef]
2. Zhang, W.; Huang, F.; Mao, K.; Lin, C.; Pan, Z. Evaluation of photovoltaic energy saving potential and investment value of urban buildings in China based on GIS technology. *Buildings* **2021**, *11*, 649. [CrossRef]
3. Alrawashdeh, H.; Stathopoulos, T. Wind loads on solar panels mounted on flat roofs: Effect of geometric scale. *J. Wind Eng. Ind. Aerod.* **2020**, *206*, 104339. [CrossRef]
4. Somekawa, D.; Taniguchi, T.; Taniike, Y. Wind loads acting on PV panels and support structures with various layouts. In Proceedings of the Eighth Asia-Pacific Conference on Wind Engineering, Chennai, India, 10–14 December 2013.
5. Stathopoulos, T.; Zisis, I.; Xypnitou, E. Local and overall wind pressure and force coefficients for solar panels. *J. Wind Eng. Ind. Aerod.* **2014**, *125*, 195–206. [CrossRef]
6. Kopp, G.A.; Farquhar, S.; Morrison, M.J. Aerodynamic mechanisms for wind loads on tilted, roof-mounted, solar arrays. *J. Wind Eng. Ind. Aerodyn.* **2012**, *111*, 40–52. [CrossRef]
7. Wang, J.X.; Yang, Q.S.; Tamura, Y. Effects of building parameters on wind loads on flat-roof-mounted solar arrays. *J. Wind Eng. Ind. Aerodyn.* **2018**, *174*, 210–224. [CrossRef]
8. Simiu, E.; Filliben, J.J. Wind direction effects on cladding and structural loads. *Eng. Struct.* **1981**, *3*, 181–186. [CrossRef]
9. Habte, F.; Chowdhury, A.G.; Yeo, D.; Simiu, E. Wind directionality factors for nonhurricane and hurricane-prone regions. *J. Struct. Eng.* **2014**, *141*, 04014208. [CrossRef]
10. ASCE/SEI 7-16. *Minimum Design Loads and Associated Criteria for Buildings and Other Structures*; American Society of Civil Engineers: Reston, VA, USA, 2016.
11. Zhang, X.; Chen, X. Influence of dependence of directional extreme wind speeds on wind load effects with various mean recurrence intervals. *J. Wind Eng. Ind. Aerodyn.* **2016**, *148*, 45–56. [CrossRef]
12. Wang, C.; Holmes, D. Exceedance rate, exceedance probability, and the duality of GEV and GPD for extreme hazard analysis. *Nat. Hazards* **2020**, *102*, 1305–1321. [CrossRef]
13. Liu, M.; Chen, X.Z.; Yang, Q.S. Estimation of multiple limit state responses with various mean recurrence intervals considering directionality effects. *J. Wind Eng. Ind. Aerodyn.* **2019**, *193*, 103959. [CrossRef]
14. Zhang, X.; Chen, X. Assessing probabilistic wind load effects via a multivariate extreme wind speed model: A unified framework to consider directionality and uncertainty. *J. Wind Eng. Ind. Aerodyn.* **2015**, *147*, 30–42. [CrossRef]
15. Chen, X. Estimation of wind load effects with various mean recurrence intervals with a closed-form formulation. *Int. J. Struct. Stab. Dy.* **2016**, *16*, 1550060. [CrossRef]
16. Payer, T.; Küchenhoff, H. Modelling extreme wind speeds at a Germanweather station as basic input for a subsequent risk analysis for high-speedtrains. *J. Wind Eng. Ind. Aerodyn.* **2004**, *92*, 241–261. [CrossRef]
17. Holmes, J.D. *Wind Loading of Structures*, 3rd ed.; CRC Press: Boca Raton, FL, USA, 2015; p. 40.
18. GB 50797-2012. *Code for Design of Photovoltaic Power Station*; Ministry of Housing and Urban-Rural Development of the People's Republic of China: Beijing, China; General Administration of Quality Supervision, Inspection and Quarantine of the People's Republic of China: Beijing, China, 2012.
19. Lieblein, J. *Efficient Methods of Extreme-Value Methodology*; Report no. NEA-CSNI-R–1976-10; Nuclear Energy Agency of the OECD (NEA): Paris, France, 1976.
20. Liu, M.; Chen, X.; Yang, Q. Estimation of Peak Factor of Non-Gaussian Wind Pressures by Improved Moment-Based Hermite Model. *J. Eng. Mech.* **2017**, *143*, 06017006. [CrossRef]
21. Yang, Q.; Chen, X.; Liu, M. Bias and Sampling Errors in Estimation of Extremes of Non-Gaussian Wind Pressures by Moment-based Translation Process Models. *J. Wind Eng. Ind. Aerodyn.* **2019**, *186*, 214–233. [CrossRef]
22. Chen, X.; Huang, G. Estimation of probabilistic extreme wind load effects: Combination of aerodynamic and wind climate data. *J. Eng. Mech.* **2010**, *136*, 747–760. [CrossRef]
23. AS/NZS 1170.2. *Structural Design Actions—Part 2: Wind Actions*; Standards Australia and Standards New Zealand: Sydney, Australia, 2011.
24. AIJ-RLB. *AIJ Recommendations for Loads on Buildings*; Architectural Institute of Japan: Tokyo, Japan, 2004.
25. Grigoriu, M. *Applied Non-Gaussian Processes: EXAMPLES, Theory, Simulation, Linear Random Vibration, and MATLAB Solutions*; Prentice-Hall: Englewood Cliffs, NJ, USA, 1995.
26. Liu, P.L.; Der Kiureghian, A. Multivariate distribution models with prescribed marginals and covariances. *Probab. Eng. Mech.* **1986**, *1*, 105–112. [CrossRef]
27. Peng, L.; Liu, M.; Yang, Q.; Huang, G.; Chen, B. An analytical formula for Gaussian to non-Gaussian correlation relationship by moment-based piecewise Hermite polynomial model with application in wind engineering. *J. Wind Eng. Ind. Aerodyn.* **2020**, *198*, 104094. [CrossRef]